2

Enhanced Motion Control Concepts on Parallel Robots

Frank Wobbe, Michael Kolbus and Walter Schumacher
Institute of Control Engineering, TU Braunschweig
Germany

1. Introduction

During the last years parallel robots have found their way into industrial applications. Though the ratio of workspace to designspace is usually worse compared to their serial counterparts, parallel robots are superior in terms of stiffness, accuracy and high-speed operation. This chapter takes the development into account and focuses on control concepts of parallel robots used for handling and assembly.

To exploit these features, an effective control system is inevitable. Since the nonlinearities of parallel structures are not negligible, control schemes have to include a precise dynamic model. This chapter presents several approaches of model-based control laws and discusses their characteristics, in theory as well as in implementation.

All discussed concepts operate on a uniform interface that takes a fully specified trajectory of position, velocity and acceleration in Cartesian space. This design of the interface can be considered as a minor restriction, since trajectories for high-speed operation usually are defined to be jerk limited (C^2-continuous) to reduce mechanical stress of the robot.

The chapter starts with a brief description of the discrete modeling scheme, afterwards a compact formulation of the robots dynamics is derived. Several control schemes using this model are presented, which can be classified into two major groups depending on the usage of the robot model as feedback or feedforward type. Based on linearization techniques the controllers for each axis are designed independently within a linear framework. The control algorithms are augmented by disturbance observers to reduce distortion of trajectory and tracking error.

Besides these classical approaches, nonlinear concepts such as sliding mode are used for control. Using a boundary layer concept and adding discontinuities to the control law ensures global asymptotic tracking with robustness against model uncertainties and disturbances. Chattering formally associated with sliding mode can be coped with modification of the control law by using continuous sliding surfaces. On contrary to the first approaches it is inherently based on nonlinear design.

Considering properties of parallel robots the control schemes of described approaches are designed. Explicit design rules are given at hand and discussed. For experiments the concepts are implemented on a planar parallel robot. The unified approaches of modeling and control guarantee transfer to more complex robots.

Evaluation of the results starts with a general comparison of control concepts. The effect of the design parameters on closed-loop system dynamics is analyzed theoretically, paying

special attention to robustness and performance as essential characteristics. To substantiate the statements of the theoretical analyses, experimental results are presented and evaluated with respect to different aspects. Cartesian distortion, tracking error, drive torques and their impact are of major concern. Finally, an overall categorization is given at hand, featuring application hints for each design concept and pointing out specific drawbacks and advantages.

2. Problem statement – control concepts on parallel robots

Robot structures based on closed kinematic chains have proven to be a promising alternative to those based on serial chains. The feature of many of these so called parallel kinematic structures to allow for the drives to be fixed to the base, is especially of great interest for the design of robots for high speed handling and assembly tasks, cf. (Merlet, 2000). It enables a design with low moving masses allowing for high accelerations and achieving shorter cycle times.

Due to the nonlinearities of the manipulator a model-based control architecture is essential to ensure precise trajectory tracking, which demands a precise and compact dynamic model. Control schemes using this model are in general mainly based on centralized, decentralized or on equivalent control (Spong & Vidyasagar, 1989), (Sciavicco & Siciliano, 2001). Whereas first schemes allow an independent design of the controllers within a linear framework, the latter is refined to sliding mode control as nonlinear design-concept, which shapes the error dynamics of the system. Moreover, control design based on linearized subsystems offers a wide range of linear control design schemes.

Due to different design aspects of these concepts specific advantages and aspects of performance can be expected, which is addressed in this article.

Specific for parallel manipulators is a complex direct kinematic problem (DKP), which is in general more complex than the inverse kinematic problem (IKP), cf. (Merlet, 2000). These demands have to be met by control design: On the one hand a precise model is needed, on the other hand the complexity is limited by computational effort in real-time operation.

3. Robot dynamics

In literature many different methods of modeling parallel robots have been proposed, based on the approaches of the Newton-Euler method on the one hand (Spong & Vidyasagar, 1989) and the Lagrangian principle on the other hand (Tsai, 1999), (Murray et al., 1994). In this paper, Lagrangian equations of the second type and the formulation of Lagrange-D'Alembert (Nakamura, 1991) will be used for obtaining a compact model, guaranteeing computational efficiency in real-time control. The core idea herein is established on the use of Jacobians for discrete modeling.

3.1 Discrete modeling

Discrete modeling of parallel structures can be divided into two major steps: Derivation of manipulators Jacobian and calculation of differential equations.

The first step is discussed in (Stachera & Schumacher, 2007) and (Stachera et al., 2007), where the calculation of Jacobians bases on cutting open the parallel structure at the endeffector and applying the principle of kineto-statics (cf. section 3.3). Jacobian matrices of

serial manipulators representing differential kinematic relation $\dot{\mathbf{x}} = \mathbf{J}\dot{\mathbf{q}}$ and static relation $\boldsymbol{\tau} = \mathbf{J}^{\mathrm{T}}\mathbf{f}$ are used for deduction.

The second step – deduction of an exact model for a given structure – can be done via Lagrange-D'Alembert-Formulation

$$\frac{\mathrm{d}}{\mathrm{d}t}\left(\frac{\partial L}{\partial \dot{\mathbf{q}}}\right) - \frac{\partial L}{\partial \mathbf{q}} = \boldsymbol{\tau} + \mathbf{J}^{\mathrm{T}}\mathbf{f}_{\mathrm{ext}} \tag{1}$$

with $L = T - V$ representing Lagrange function, T kinetic energy, V potential energy, $\mathbf{q}$ vector of joint space variables, $\boldsymbol{\tau}$ actuator torques and $\mathbf{J} = \mathbf{G}^{+\mathrm{T}}$ serial manipulator Jacobian on which external forces $\mathbf{f}_{\mathrm{ext}}$ are applied. Computing energy functions

$$T = \frac{1}{2}\dot{\mathbf{q}}^{\mathrm{T}}\mathbf{M}_{\mathbf{q}}(\mathbf{q})\dot{\mathbf{q}} \quad , \quad V = \int_{\mathbf{q}_0}^{\mathbf{q}} \boldsymbol{\eta}_{\mathbf{q}}(\mathbf{q})\,\mathrm{d}\mathbf{q} \tag{2}$$

leads to a differential equation in joint space coordinates:

$$\mathbf{M}_{\mathbf{q}}(\mathbf{q})\ddot{\mathbf{q}} + \mathbf{C}_{\mathbf{q}}(\dot{\mathbf{q}},\mathbf{q})\dot{\mathbf{q}} + \boldsymbol{\eta}_{\mathbf{q}}(\mathbf{q}) = \boldsymbol{\tau} + \mathbf{J}^{\mathrm{T}}\mathbf{f}_{\mathrm{ext}} \tag{3}$$

Its elements can be calculated, considering a discrete model; the main idea is based upon discrete point masses m_i: Starting with the simple case of planar structures each link can be replaced by a combination of at least three single point masses without neglecting and disturbing properties concerning mass, center of mass and moment of inertia, thus guaranteeing correct dynamical behavior (Dizioglu, 1966). Without loss of generality this concept can be transferred to more complex structures. With growing complexity in structure the number of discrete elements increases, resulting in the finite element method. The concept of discrete point masses leads to

$$\begin{aligned} \mathbf{M}_{\mathbf{q}} &= \sum_i m_i \mathbf{J}_i^{\mathrm{T}}\mathbf{J}_i + \mathrm{diag}\{I_m, I_m\} \\ \mathbf{C}_{\mathbf{q}} &= \frac{\partial \mathbf{M}_{\mathbf{q}}}{\partial t} - \frac{1}{2}\frac{\partial(\dot{\mathbf{q}}^{\mathrm{T}}\mathbf{M}_{\mathbf{q}})}{\partial \mathbf{q}} \\ \boldsymbol{\eta}_{\mathbf{q}} &= \sum_i m_i \mathbf{J}_i^{\mathrm{T}}\mathbf{g} \end{aligned} \tag{4}$$

with drive inertia I_m and $\mathbf{g}$ being vector of gravity. All Jacobians $\mathbf{J}_i$ can be described by a linear combination of endeffector- and passive joints Jacobians.

The choice of Coriolis-Matrix is not unique: Using Christoffel-Symbols and following the notation of (Vetter, 1973) and (Weinmann, 1991) with discussion in (Bohn, 2000) leads to

$$\mathbf{C}_{\mathbf{q}} = \frac{1}{2}\left\{\left(\dot{\mathbf{q}}^{\mathrm{T}} \otimes \mathbf{I}_{n_{\mathbf{q}}}\right) - \left(\mathbf{I}_{n_{\mathbf{q}}} \otimes \dot{\mathbf{q}}^{\mathrm{T}}\right)\right\}\frac{\partial \mathbf{M}_{\mathbf{q}}}{\partial \mathbf{q}} + \frac{1}{2}\left\{\left(\mathbf{I}_{n_{\mathbf{q}}} \otimes \dot{\mathbf{q}}^{\mathrm{T}}\right)\frac{\partial \mathbf{M}_{\mathbf{q}}}{\partial \mathbf{q}}\right\}^{\mathrm{T}} \tag{5}$$

where $\otimes$ denotes the Kronecker-product, $n_{\mathbf{q}}$ is the number of degrees of freedom of the parallel structure and

$$\frac{\partial \mathbf{M_q}}{\partial \mathbf{q}} = m_i \frac{\partial\left(\mathbf{J}_i^{\mathrm{T}}\mathbf{J}_i\right)}{\partial \mathbf{q}} = \frac{\partial \mathbf{J}_i^{\mathrm{T}}}{\partial \mathbf{q}}\mathbf{J}_i + \left(\mathbf{I}_{n_{\mathbf{q}}} \otimes \mathbf{J}_i^{\mathrm{T}}\right)\frac{\partial \mathbf{J}_i}{\partial \mathbf{q}} \tag{6}$$

A basic feature of this rearranging is skew-symmetry of $\dot{\mathbf{M}}_{\mathbf{q}} - 2\mathbf{C}_{\mathbf{q}}$, e.g.

$$\mathbf{w}^{\mathrm{T}}\left(\dot{\mathbf{M}}_{\mathbf{q}} - 2\mathbf{C}_{\mathbf{q}}\right)\mathbf{w} = 0 \quad , \qquad \mathbf{w} \in \Re^{\left(n_{\mathbf{q}} \times 1\right)} \tag{7}$$

which simplifies matrix usage for control algorithms (Sciavicco & Siciliano, 2001).
Without loss of generality this formalism can be enhanced for more complex structures featuring elasticities or redundancies. It thus can be used for generalized parallel structures considering an adequate discrete mass distribution.

3.2 Dynamics equations

Control in operational space requires coordinate transformation, resulting in

$$\mathbf{M_x}(\mathbf{q})\ddot{\mathbf{x}} + \mathbf{C_x}(\dot{\mathbf{q}},\mathbf{q})\dot{\mathbf{x}} + \boldsymbol{\eta}_{\mathbf{x}}(\mathbf{q}) = \mathbf{G}\boldsymbol{\tau} + \mathbf{f}_{\mathrm{ext}} \tag{8}$$

with

$$\begin{aligned}
\mathbf{M_x} &= \mathbf{J}^{-\mathrm{T}}\mathbf{M_q}\mathbf{J}^{-1} = \mathbf{G}\mathbf{M_q}\mathbf{G}^{\mathrm{T}} \\
\mathbf{C_x} &= \mathbf{J}^{-\mathrm{T}}\left(\mathbf{C_q}\mathbf{J}^{-1} + \mathbf{M_q}\dot{\overline{\mathbf{J}^{-1}}}\right) = \mathbf{G}\left(\mathbf{C_q}\mathbf{G}^{\mathbf{T}} + \mathbf{M_q}\dot{\mathbf{G}}^{\mathrm{T}}\right) \\
\boldsymbol{\eta}_{\mathbf{x}} &= \mathbf{J}^{-\mathrm{T}}\boldsymbol{\eta}_{\mathbf{q}} = \mathbf{G}\boldsymbol{\eta}_{\mathbf{q}}
\end{aligned} \tag{9}$$

where (7) still holds. Matrix-dependence on joint space variables can be noted as advantageous. These are measured and used for computation of the direct kinematic problem (DKP).

3.3 Planar parallel manipulator FIVEBAR

For experimental setup a planar parallel structure with $n_{\mathbf{q}} = 2$ degrees of freedom, named FIVEBAR (cf. fig. 1), is used. The end effector of the manipulator is connected to the drives by two independent kinematic chains. Cranks and rods of the manipulator are made of carbon fiber to reduce the weight of moved masses, thus being well-suited for high-speed operation with a maximum velocity *v = 5 m/s* and acceleration *a = 70 m/s²* in Cartesian space. The control system consists of a PC running QNX and an IEEE 1394 FireWire link to the inverters ensuring short cycle time and sufficient bandwidth for control purposes.
Applying deduced discrete modeling scheme requires determination of manipulators Jacobian, which can be calculated via internal link forces $\mathbf{f}_{\mathrm{B}} = \begin{bmatrix} f_{\mathrm{B}_1} & f_{\mathrm{B}_2} \end{bmatrix}^{\mathrm{T}}$. Use of static relations of the end effector results in

$$\mathbf{f}_{\mathrm{B}} = \begin{bmatrix} s_1 & s_2 \end{bmatrix}^{-1}\mathbf{f}_{\mathrm{ext}} = \mathbf{S}^{-1}\mathbf{f}_{\mathrm{ext}} \tag{10}$$

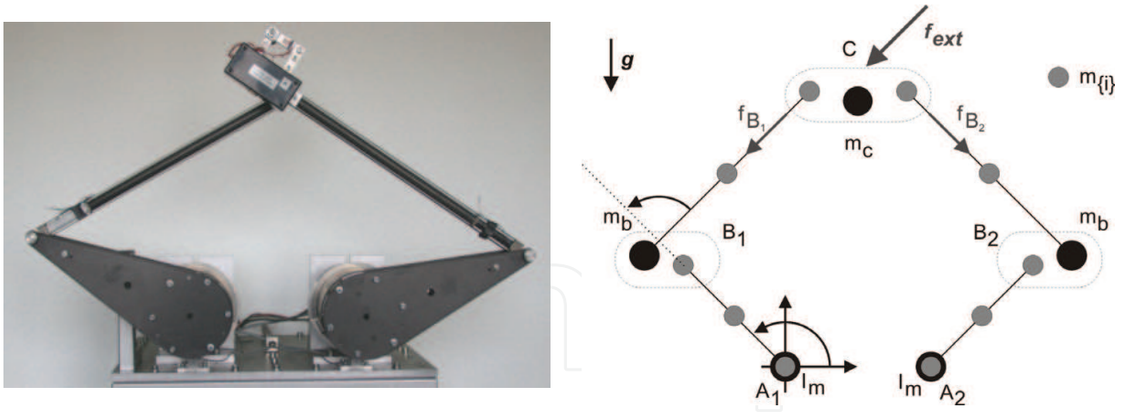

Fig. 1: Planar parallel manipulator FIVEBAR and its discrete model

Considering that the links connected to the end effector do not transmit transverse forces (no elasticities featured), the Jacobian of the end effector point *C* can be deduced as

$$\mathbf{G}^{+} = \operatorname{diag}\left\{\mathbf{J}_{B_1}, \mathbf{J}_{B_2}\right\}^{T} \operatorname{diag}\left\{\mathbf{s}_1, \mathbf{s}_2\right\}\mathbf{S}^{-1} = \mathbf{J}_C^{T} = \mathbf{J}^{T} \tag{11}$$

representing the Jacobian of the parallel manipulator. Moreover, Jacobians of passive joints can be determined via analytical differentiation of passive joint position in operational space, which enables calculation of all other Jacobians as a linear combination. Hence the discrete modeling scheme can be applied.

4. Control design

Control design is based on a torque driven interface to the inverters at bottom layer. Its concepts first and foremost aim at tracking a trajectory specified by position, velocity and acceleration $\left\{\mathbf{x}_{\text{ref}}, \dot{\mathbf{x}}_{\text{ref}}, \ddot{\mathbf{x}}_{\text{ref}}\right\}$ in the base frame of the robot.

In general two different approaches for design of the subordinated drive-controller can be noted: linear control concepts based upon linearization techniques on the one hand and nonlinear ones such as sliding mode control on the other hand. Both provide a uniform trajectory interface for the top layer, which ensures hybrid control within the task-frame formalism, as discussed in (Kolbus et al., 2005), (Finkemeyer, 2004). Thus the manipulator is not restricted to position control, but extendable to force control in operational space.

4.1 Linearization techniques: Feedback vs. Feedforward

Classical linear control concepts can be applied, if linearization techniques are used. These can be distinguished between exact feedback linearization and computed torque feedforward linearization (Isidori, 1995), (Spong & Vidyasagar, 1989), (Sciavicco & Siciliano, 2001).

The implementation of the inverse dynamic control is illustrated in fig. 2 where the manipulator is assumed to be nonredundant. In case of redundancy the principle remains the same, where additional actuator degrees of freedom can be used for internal pre-stressing of mechanical structure (Kock, 2001). The model derived in section 3 is used to set the input to

$$\boldsymbol{\tau} = \mathbf{G}^{-1}\mathbf{M}_{\mathbf{x}}\mathbf{u} + \mathbf{G}^{-1}\boldsymbol{\xi}_{\mathbf{x}}, \quad \boldsymbol{\xi}_{\mathbf{x}} = \mathbf{C}_{\mathbf{x}}\dot{\mathbf{x}} + \boldsymbol{\eta}_{\mathbf{x}} \tag{12}$$

where **u** is the new external reference input. Its basic feature is the use of measured values for linearization. Equation (12) renders the closed loop dynamical behavior of the overall system to a set of decoupled double integrators in Cartesian space.
Computed torque feedforward linearization to the contrary uses reference values instead of measured values. In implementation (cf. fig. 3) derived model is used to calculate the input as

$$\boldsymbol{\tau} = \mathbf{G}^{-1}\mathbf{M}_{\mathbf{x}}\ddot{\mathbf{x}}_{\mathrm{ref}} + \mathbf{G}^{-1}\boldsymbol{\xi}_{\mathbf{x},\mathrm{ref}} + \mathbf{M}_{\mathbf{q}}\mathbf{v}\,, \quad \boldsymbol{\xi}_{\mathbf{x},\mathrm{ref}} = \mathbf{C}_{\mathbf{x}}\dot{\mathbf{x}}_{\mathrm{ref}} + \boldsymbol{\eta}_{\mathbf{x}}\,, \quad \mathbf{M}_{\mathbf{q}} = \mathbf{G}^{-1}\mathbf{M}_{\mathbf{x}}\mathbf{G}^{-\mathrm{T}} \tag{13}$$

where **v** represents the new reference input, analogues to exact feedback linearization. A set of double integrators is obtained by eq. (13) for closed loop dynamics, this time, however, in joint space.

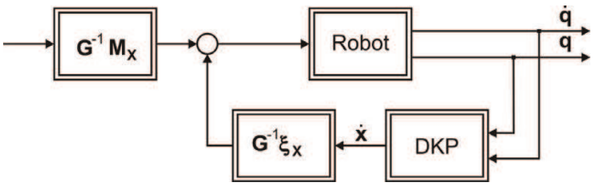

Fig. 2: Feedback linearization

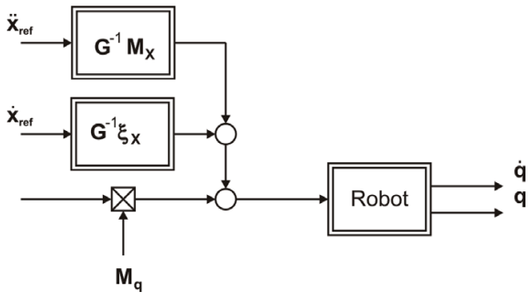

Fig. 3: Feedforward linearization

The delay of the inverters affects the described linearization. Instead of a set of double integrators, feedback (eq. (12)) and feedforward linearization (eq. (13)) results in

$$T_{\mathrm{v}}u_i = T_{\mathrm{el}}x_i^{(3)} + x_i^{(2)}\,, \quad T_{\mathrm{v}}v_i = T_{\mathrm{el}}q_i^{(3)} + q_i^{(2)}\,, \quad i \in \{1,\ldots,n_{\mathbf{q}}\} \tag{14}$$

as description for the linearized subsystem, respectively, where T_{el} denotes the delay of the inverter and T_{v} represents the virtual inertia of the linearized mechanical system. In absence of model uncertainties linearization techniques yield $T_{\mathrm{v}} = 1$. Nonlinear terms have been neglected here, but are taken into account as disturbances for the design of the top layer axis controller.
Comparing both concepts reveals important aspects: Whereas feedback linearization results in control in operational space, e.g. centralized control, feedforward linearization leads to decentralized control in joint space. The fact, that in general for parallel structures the IKP is easier to solve than the DKP, suggests the use of computed torque feedforward linearization for parallel manipulators. The advantage of feedback linearization on the other hand is the decoupling of axes – single controllers do not compete.
In case of FIVEBAR the direct kinematic problem is of nearly the same complexity as the inverse one, thus both concepts will be shown.

4.2 Linear cascaded control schemes: Centralized vs. Decentralized

Based upon linearization techniques described in former section, cascaded control schemes can be developed. Following (Sciavicco & Siciliano, 2001) due to their difference in linearization, they can be denoted as centralized control in case of feedback linearization on the one hand and decentralized control or computed torque control on the other hand.

Design is based upon the linearized subsystem given by eq. (14), resulting in a cascaded control scheme, see fig 4. and fig. 5.

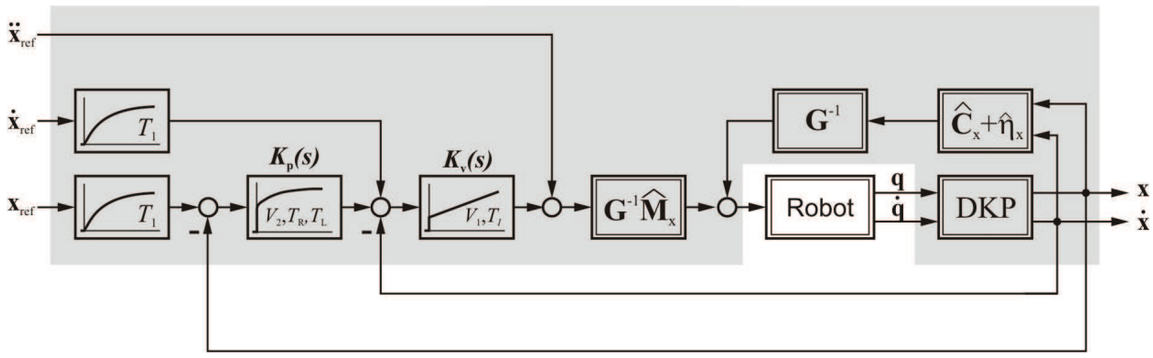

Fig. 4: Cascade control / centralized control

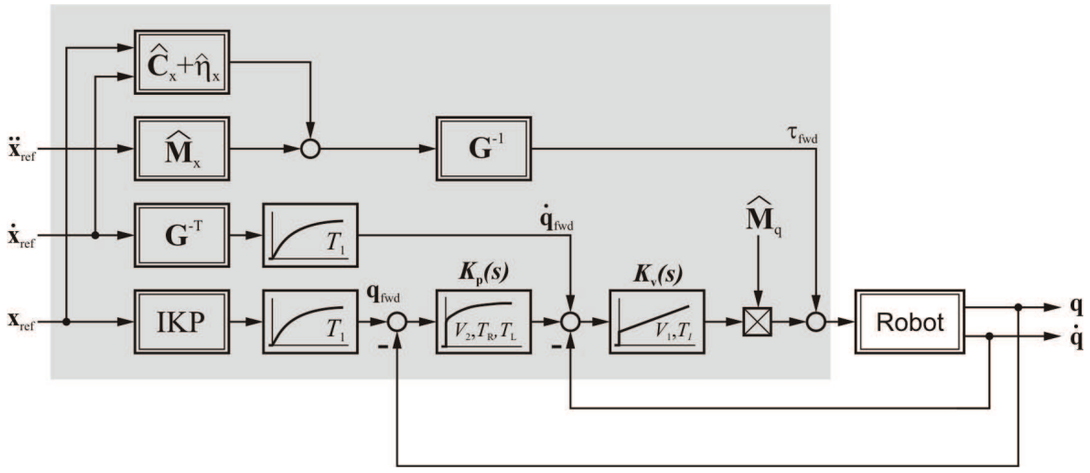

Fig. 5: Computed torque control / decentralized control

The control laws – common for both control schemes – are described by transfer functions

$$K_v(s) = V_1 \frac{T_i s + 1}{T_i s}, \quad K_p(s) = V_2 \frac{T_R s + 1}{T_L s + 1} \tag{15}$$

The parameters can be derived by symmetrical optimum design (Leonhard, 1996), which maximizes the phase margin of control system and ensures stability in presence of model uncertainties. The inherent overshoot of the velocity controller needs to be compensated by the outer loop. Therefore, a simple proportional control law is insufficient and replaced by a PTD-controller that suppresses the overshot and offers better performance. By using the damping $D_p = D_v = 1$ as parameter for closed loop design of velocity- and position-cascade one obtains

$$\begin{aligned} V_1 &= \frac{1}{3T_{\mathrm{el}}}, \quad T_i = 9T_{\mathrm{el}} \\ V_2 &= \frac{4}{81T_{\mathrm{el}}}, \quad T_R = 3T_{\mathrm{el}}, \quad T_L = T_i \end{aligned} \tag{16}$$

A more detailed discussion can be found in (Leonhard, 1996).
Alternatively, parameters can be determined by comparing the denominator of the closed loop dynamics with a model function. The damping D of one complex pole pair can be chosen independently and all other poles are placed on real axis. Following the idea of minimizing the integral of disturbance step response, the parameters are obtained as

$$\begin{aligned} V_1 &= \frac{5D^2+1}{16D^2T_{\mathrm{el}}}, & T_i &= \frac{4T_{\mathrm{el}}(5D^2+1)}{1+2D^2} \\ V_2 &= \frac{1}{4T_{\mathrm{el}}(1+2D^2)}, & T_R &= 4T_{\mathrm{el}}, & T_L &= T_i \end{aligned} \tag{17}$$

which is discussed more widely in (Brunotte, 1999).
Whereas first design aims at maximizing phase margin and therefore targets robustness, the second one tends to optimize feedforward dynamics and disturbance rejection. The second design is preferable on parallel robots due to their high accelerations.

4.3 Disturbance observer based control

To improve disturbance rejection the concept of disturbance observers is well known in literature. This method focuses on observing disturbances and using them as a feedforward signal. A special concept, the principle of input balancing as introduced by (Brandenburg & Papiernik, 1996) offers advantages on tracking as well as disturbance rejection. Its core idea consists of a direct feed-through in forward control amended by a disturbance observer. In contrast to classical observers (Luenberger, 1964), (Lunze, 2006) this principle uses the controlled velocity plant as model for observing disturbances, which leads to an improvement in command action with improved robustness against external disturbances. Formerly intended for linear systems the linearization techniques presented in section 4.1 ensure using input balancing for robot control. Based on the linearized subsystem given by eq. (14) the control structure is illustrated in fig. 6.

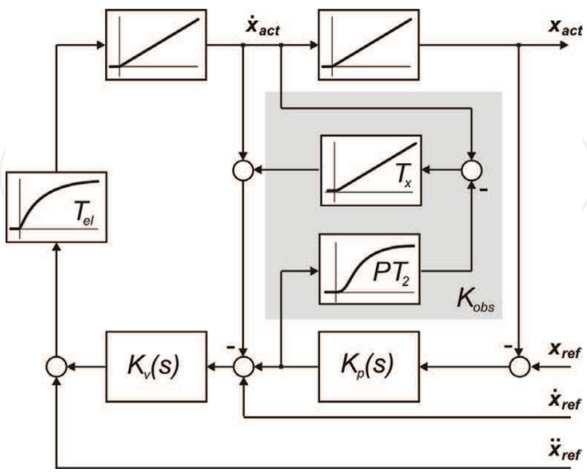

Fig. 6: Input balancing with centralized control

For computed torque control operational space references and measured values have to be replaced by joint space variables.

The control laws are described by transfer functions

$$\begin{aligned} K_v(s) &= V_1, & K_p(s) &= V_2 \\ K_{PT_2}(s) &= \frac{1}{\left(\frac{s}{\omega_0}\right)^2 + \frac{2D_v}{\omega_0}s + 1}, & K_x(s) &= \frac{1}{T_x s} \end{aligned} \tag{18}$$

Here $K_{PT_2}(s)$ represents the model of the closed loop velocity cascade, the disturbance-model is matched by an integrator $K_x(s)$. Using $D_p = 1$ for damping in position control loop leads to parameters

$$\begin{aligned} V_1 &= \frac{1}{3T_{\mathrm{el}}}, & V_2 &= \frac{1}{9T_{\mathrm{el}}} \\ \frac{2D_v}{\omega_0} &= 3T_{\mathrm{el}}, & \frac{1}{\omega_0^2} &= 3T_{\mathrm{el}}^2, \quad T_x = 9T_{\mathrm{el}} \end{aligned} \tag{19}$$

for control.
Using this control concept, an improvement in trajectory tracking compared to classical cascaded control schemes can be expected – due to the observer. On the other hand model uncertainties nonetheless have impact on the dynamical behavior (Wobbe et. al., 2006).

4.4 Sliding mode control

An approach to address an uncertain model is sliding mode control. The basic concept has been discussed by (Utkin, 1977) and was taken up by (Slotine, 1983) with a general definition of sliding surfaces and boundary layers to lessen the effect of chattering. This section focuses on control via sliding mode of first order, see fig. 7 – an extension to higher order sliding modes to reduce chattering can be found in the works of (Levant & Friedman, 2002).

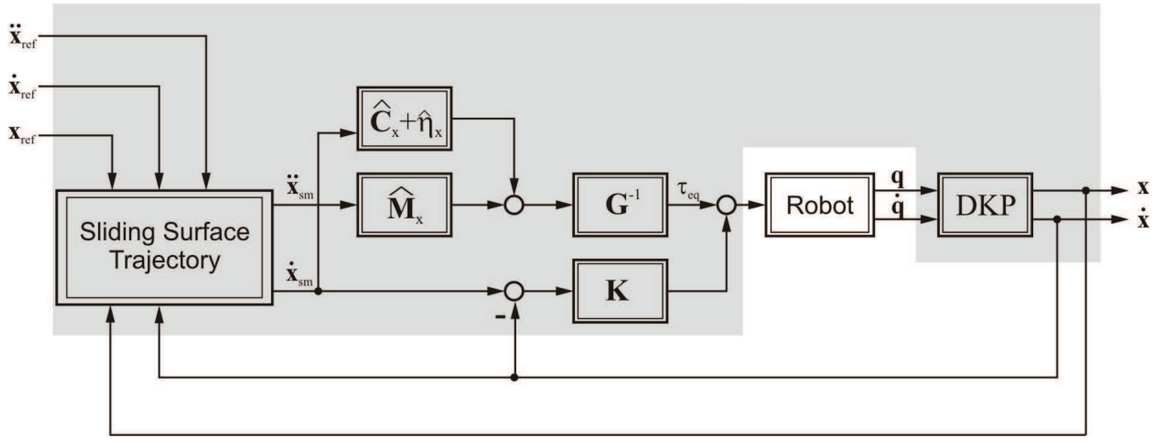

Fig. 7: Sliding mode control using continuous sliding surfaces

On contrary to linear design concepts as cascade control and input balancing sliding mode control is based on nonlinear design and focuses on the dynamics of the tracking-error (Wobbe et al., 2007), considered and defined by a sliding surface

$$\mathbf{s} = \dot{\tilde{\mathbf{x}}} + \mathbf{\Lambda}\tilde{\mathbf{x}}\,, \quad \tilde{\mathbf{x}} = \mathbf{x}_{\mathrm{act}} - \mathbf{x}_{\mathrm{ref}} \tag{20}$$

with a positive definite matrix $\mathbf{\Lambda}$. The error is restricted to the sliding surface by modifying the reference trajectory and computing a virtual trajectory $\{\mathbf{x}_{\mathrm{sm}}, \dot{\mathbf{x}}_{\mathrm{sm}}, \ddot{\mathbf{x}}_{\mathrm{sm}}\}$ with

$$\mathbf{x}_{\mathrm{sm}} = \mathbf{x}_{\mathrm{ref}} - \mathbf{\Lambda}\int_0^t \tilde{\mathbf{x}}\,\mathrm{d}\,t \tag{21}$$

This trajectory definition is used for the computation of the control law under use of equivalent dynamics set point $\boldsymbol{\tau}_{\mathrm{eq}}$ in Filippov's sense (Slotine & Li, 1991), (Filippov, 1988)

$$\boldsymbol{\tau} = \boldsymbol{\tau}_{\mathrm{eq}} - \mathbf{u} = \mathbf{G}^{-1}(\hat{\mathbf{M}}_{\mathbf{x}}\ddot{\mathbf{x}}_{\mathrm{sm}} + \hat{\mathbf{C}}_{\mathbf{x}}\dot{\mathbf{x}}_{\mathrm{sm}} + \hat{\boldsymbol{\eta}}_{\mathbf{x}}) - \mathbf{K}\mathbf{s} \tag{22}$$

where $\hat{\mathbf{M}}_{\mathbf{x}}$, $\hat{\mathbf{C}}_{\mathbf{x}}$ and $\hat{\boldsymbol{\eta}}_{\mathbf{x}}$ denote estimates of manipulator dynamics. The additional input $\mathbf{u}$ ensures stability and precise tracking in the presence of model uncertainties. It copes chattering formally associated with sliding mode control by the continuous sliding surface. The control law features no discontinuities such as switching terms. The reduced tendency of chattering is gained at the price of slightly reduced – but still outstanding – performance compared to original switching concept.
The performance of control by sliding surfaces depends on matrix $\mathbf{\Lambda}$ with the delay of the inverter being its most limiting factor. Thus parameters of sliding mode control are obtained by

$$\mathbf{\Lambda} = \frac{1}{3T_{\mathrm{el}}}\begin{bmatrix} 1 & 0 \\ 0 & 1 \end{bmatrix}, \quad \mathbf{K} = \mathbf{G}^{-1}\hat{\mathbf{M}}_{\mathbf{x}}\mathbf{\Lambda} \tag{23}$$

An improvement in performance can be obtained by focusing on the integral of tracking error. Redefinition of the corresponding sliding surface

$$\mathbf{s} = \ddot{\tilde{\mathbf{x}}} + 2\mathbf{\Lambda}\dot{\tilde{\mathbf{x}}} + \mathbf{\Lambda}^2\int_0^t \tilde{\mathbf{x}}\,\mathrm{d}\,t \tag{24}$$

forces integral action and thus improves disturbance rejection.

5. Comparison of control concepts

Presented design concepts feature different characteristics. As essential among others the performance of feedforward-dynamic, i.e. command action on the one hand and the robustness against parameter variation, i.e. disturbance rejection are paid special attention, revealing hints for range of application. Theoretical analysis here is based on the closed loop dynamics considering applied linearization techniques.

5.1 Performance

Performance of control concepts can be subdivided into groups: the linearization technique and closed loop system dynamics of an equivalent linear system.

Referring to linearization three different methods have been presented: decentralized, centralized and equivalent control. Performance analysis is widely spread in literature (Whitcomb et al., 1993), (Slotine, 1985) and kept rather short for sake of simplicity. Main characteristics are – referring to weak points of each technique – an influence of measurement noise for centralized control, drift of linearization in case of trajectory following error in decentralized control and both – however to a far lesser extend – for equivalent control.

Closed loop system dynamics reveal different aspects on command action and disturbance rejection, see tab.1

	Cascade (1)	Cascade (2)	Input balancing
FF	$\frac{4}{(9T_{el}s+1)^2(9T_{el}s+4)}$	$\frac{1}{(4T_{el}s+1)^3}$	$\frac{1}{(3T_{el}s+1)^3}$
DIST	$\frac{2187T_{el}^3s(T_{el}s+1)}{(9T_{el}s+1)^2(9T_{el}s+4)(3T_{el}s+1)}$	$\frac{256T_{el}^3s(T_{el}s+1)}{(4T_{el}s+1)^4}$	$\frac{243T_{el}^3s(T_{el}s+1)(3T_{el}^2s^2+3T_{el}s+1)}{(3T_{el}s+1)^6}$

Tab. 1: Closed Loop Dynamics – Feedforward (FF) and Disturbance (DIST) of linear control schemes

Input balancing offers a good bandwidth for command action, firstly presented control design for cascade control (1) ranging up to 33% compared to this, which can be optimized up to 75% with optimized parameters (2). Static disturbances are rejected by each control scheme, with optimized cascade control providing good damping – outperformed just slightly by input balancing.

Sliding mode control in comparison to linear control schemes possesses nonlinear closed loop dynamics that can be subdivided into two parts. In case of absence of disturbances and model uncertainties, its dynamics are described by sliding, i.e. referring to eq. (20) and (24) the system output error $\tilde{\mathbf{x}}$ exponentially – with time constant $\frac{1}{\lambda}$ ($\frac{2}{\lambda}$ in case of integral action) – slides to zero. The system dynamics are matched by dynamics on the sliding surface. In case of disturbances, model uncertainties or improper initial conditions, additional dynamics are present, describing the reaching phase towards the sliding surface. Its convergence mainly depends on **K**, considering eq. (23) leads to a time constant $\frac{1}{\lambda}$.

The overall dynamics in case of disturbances **d** can thus be described by

$$\mathbf{M_x}\ddot{\tilde{\mathbf{x}}} + (2\mathbf{M_x}\mathbf{\Lambda} + \mathbf{C_x})\dot{\tilde{\mathbf{x}}} + (\mathbf{M_x}\mathbf{\Lambda} + \mathbf{C_x})\mathbf{\Lambda}\tilde{\mathbf{x}} = \mathbf{d} \tag{25}$$

for classical sliding mode control and

$$\mathbf{M_x}\dddot{\tilde{\mathbf{x}}} + (3\mathbf{M_x}\mathbf{\Lambda} + \mathbf{C_x})\ddot{\tilde{\mathbf{x}}} + (3\mathbf{M_x}\mathbf{\Lambda} + 2\mathbf{C_x})\mathbf{\Lambda}\dot{\tilde{\mathbf{x}}} + (\mathbf{M_x}\mathbf{\Lambda} + \mathbf{C_x})\mathbf{\Lambda}^2\tilde{\mathbf{x}} = \dot{\mathbf{d}} \tag{26}$$

for sliding mode control with integral action. For sake of simplicity inverter dynamics have been neglected. A consideration can be found in (Levant & Friedman, 2002) showing that dynamics are pushed to sliding of order two with similar dynamics.
Comparing sliding mode to linear control design reveals an offset in disturbance rejection for classical sliding mode control, which can be coped with integral action, cf. eq. (25) and (26). It can be seen that chosen parameters lead to similar closed loop dynamics as input balancing, however being nonlinear.

5.2 Robustness against model uncertainties

Robustness of the selected control scheme is an important issue when dealing with parallel robots. The control concepts that base on linearization techniques use an underlying linear controller to compensate model uncertainties and reject disturbances. Considering the control laws introduced in section 4 each drive is treated individually. Important system parameters for controller design are the inertia of the mechanical system T_v and the delay introduced by the inverter and communication T_el, cf. eq. (14).

The virtual inertia comprises the drive and parts of the structure. Although compensated by both linearization concepts, it varies in case of model uncertainties and payload changes. Considering the structure of the cascaded controller, as introduced in fig. 4 and 5, the transfer function for command action yields to

$$G_c(s) = \frac{G_\mathrm{PTD}G_\mathrm{PI}G_\mathrm{I1}G_\mathrm{PT1}G_\mathrm{I2}}{1 + G_\mathrm{PI}G_\mathrm{I1}G_\mathrm{PT1} + G_\mathrm{PTD}G_\mathrm{PI}G_\mathrm{I1}G_\mathrm{PT1}G_\mathrm{I2}} \tag{27}$$

The parameter uncertainties are included by an additional factor to the properties. The systems inertia and delay are thus described by $k_\mathrm{Tel}T_\mathrm{el}$ and $k_\mathrm{Tv}T_\mathrm{v}$, where T_el and T_v represent the values used for controller design. Thus, the transfer function, eq. (27), can be simplified by using eq. (17) to

$$\begin{aligned} G_C(s) &= \frac{4T_\mathrm{el}s + 1}{256T_\mathrm{el}^4 k_\mathrm{Tv}k_\mathrm{Tel}s^4 + 256T_\mathrm{el}^3 k_\mathrm{Tv}s^3 + 96T_\mathrm{el}^2 s^2 + 16T_\mathrm{el}s + 1} \\ &= \frac{a+1}{k_\mathrm{Tel}k_\mathrm{Tv}a^4 + 4k_\mathrm{Tv}a^3 + 6a^2 + 4a + 1} \end{aligned} \tag{28}$$

To avoid the explicit solution of the fourth-order polynomial, the stability of the loop is analyzed using Hurwitz' criteria. This yields to the determinant of the matrix

$$\left|\mathbf{H}_3\right| = \begin{vmatrix} 256T_\mathrm{el}^3 k_\mathrm{Tv} & 16T_\mathrm{el} & 0 \\ 256T_\mathrm{el}^4 k_\mathrm{Tv}k_\mathrm{Tel} & 96T_\mathrm{el}^2 & 1 \\ 0 & 256T_\mathrm{el}^3 k_\mathrm{Tv} & 16T_\mathrm{el} \end{vmatrix} = 2^{16}T_\mathrm{el}^6 k_\mathrm{Tv}\left(6 - k_\mathrm{Tel}\right) \tag{29}$$

The inequalities derived from the matrix are linearly dependent. To ensure stability there is no limitation to factor k_Tv, whereas the variation of the delay T_el is restricted by

$$\left|\mathbf{H}_3\right| > 0 \Leftrightarrow 6 - k_{\mathrm{Tel}} > 0 \Leftrightarrow k_{\mathrm{Tel}} < 6 \tag{30}$$

which is illustrated in fig. 10. Besides stability, dynamic behavior of the control structure is important. It is analyzed by the root locus of the system. Eq. (28) shows the general structure of denominator. The pole placement is independent of T_{v} and scaled by the delay T_{el}. Thus, the location of the poles with respect to the parameters k_{Tel} and k_{Tv} is examined in a normalized diagram. The results are shown in fig 8.

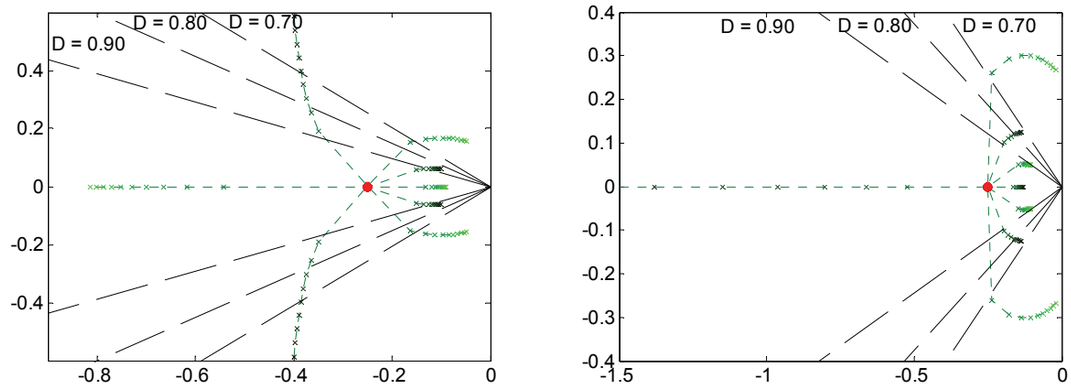

Fig. 8: Map of poles. Left: Mass is varied, right: Variation of delay. Green indicates that the real value is larger then that used for controller design. The red dot marks the location in case of no variation.

Since the factors k_{Tel} and k_{v} are linearly scaled the plots reveal the sensitivity to parameter variation. The actual damping of the outer loop is affected heavily by parameter mismatch. The step response in fig. 9 illustrates the performance loss. Errors in the delay are again more critical.

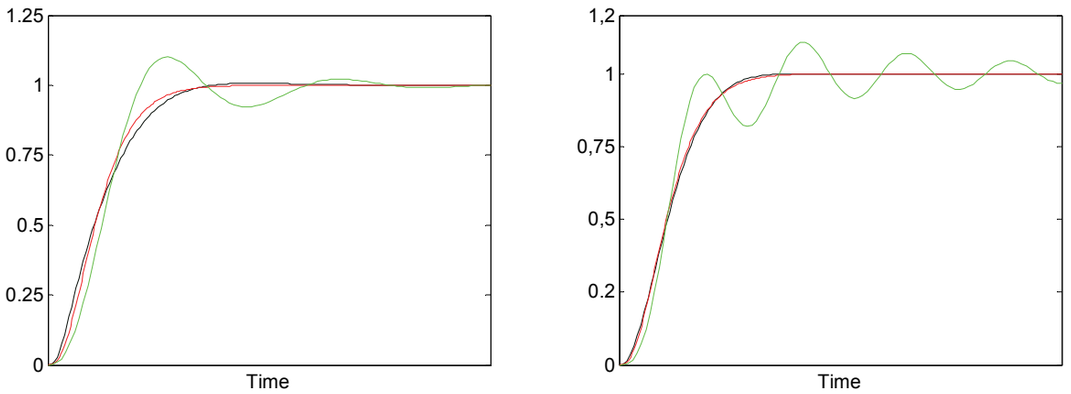

Fig. 9: Step response of closed loop. Left: Variation of mass. Right: Variation of delay. The response with correct parameters is plotted in red. Green indicates that the real value is larger then that used for controller design, black marks the opposite.

Assuming parameter variation in case of input balancing the transfer function can be expressed by

$$G_{\mathrm{IB}}(s) = \frac{a^3 + 3a^2 + 3a + 1}{k_{\mathrm{Tv}}k_{\mathrm{Tel}}a^6 + 3k_{\mathrm{Tv}}(1+k_{\mathrm{Tel}})a^5 + 3(1+k_{\mathrm{Tv}}k_{\mathrm{Tel}}+3k_{\mathrm{Tv}})a^4 + (3k_{\mathrm{Tv}}+11)a^3 + 15a^2 + 6a + 1} \tag{31}$$

where $a = 3T_{\mathrm{el}}s$ and controller parameters are set according to eq. (19). Though, the relative degree of the system is still three, no poles and zeros are cancelled out, which leads to a more complex dynamic. The stability limits are analyzed by Hurwitz criteria again

$$\mathbf{H}_5 = \begin{bmatrix} 3k_{\mathrm{Tv}}(1+k_{\mathrm{Tel}}) & 9k_{\mathrm{Tv}}+11 & 6 & 0 & 0 \\ k_{\mathrm{Tv}}k_{\mathrm{Tel}} & 3(1+k_{\mathrm{Tv}}k_{\mathrm{Tel}}+3k_{\mathrm{Tel}}) & 15 & 1 & 0 \\ 0 & 3k_{\mathrm{Tv}}(1+k_{\mathrm{Tel}}) & 9k_{\mathrm{Tv}}+11 & 6 & 0 \\ 0 & k_{\mathrm{Tv}}k_{\mathrm{Tel}} & 3(1+k_{\mathrm{Tv}}k_{\mathrm{Tel}}+3k_{\mathrm{Tel}}) & 15 & 1 \\ 0 & 0 & 3k_{\mathrm{Tv}}(1+k_{\mathrm{Tel}}) & 9k_{\mathrm{Tv}}+11 & 6 \end{bmatrix} \tag{32}$$

$$\left|\mathbf{H}_i\right| > 0, i \in \{2,3,4,5\}, \text{where } \mathbf{H}_i \text{ are the upper left submatrices of } \mathbf{H}_5$$

Due to the high system order several inequalities have to be taken into account that lead to the stability area shown in fig. 10. Compared to cascade control input balancing tolerates lesser parameter uncertainties. Moreover, stability depends on the accuracy of inertia, mirrored in parameter k_{Tv}, as well.

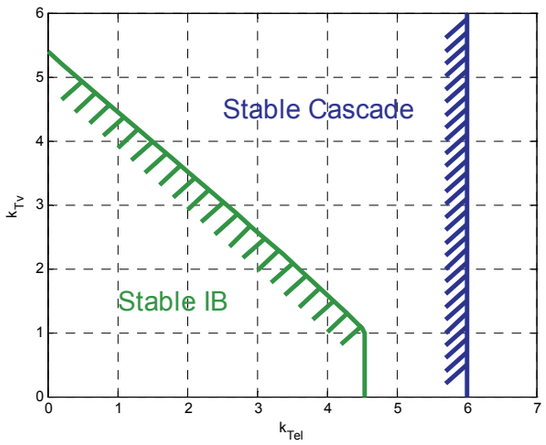

Fig. 10: Stability of linear control schemes dependent on variation

The pole-zero map of the transfer function, eq (31), is presented in fig. 11. Both parameters, inertia and delay, have significant impact on system dynamics. In line with cascade control scheme input balancing is more sensitive to variations, when parameters are assumed smaller than in reality. This is substantiated by the step response of the system, see fig. 12, which points out the lack of damping in case of wrong parameters. Both step responses (fig. 9, 12) are computed with the same parameter mismatch.

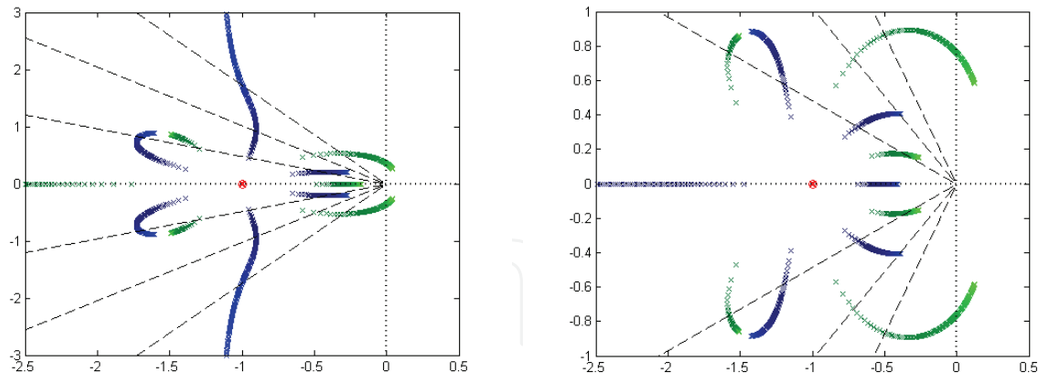

Fig 11: Map of poles. Left: Mass is varied, right: Variation of delay. Green indicates that the real value is greater than that used for controller design, whereas blue marks the opposite. The red dot marks the location in case of no variation. The dashed line indicates the damping cone for D=0.9, D=0.7 and D=0.5, respectively.

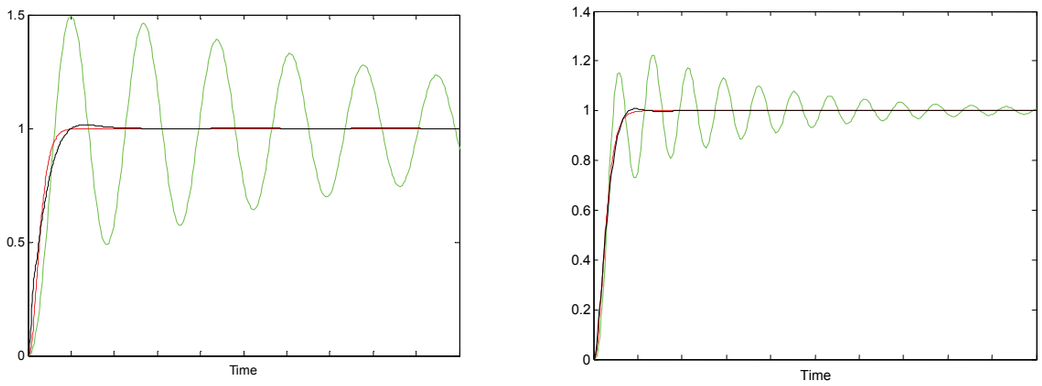

Fig. 12: Step response of closed loop (input balancing). Left: Variation of mass. Right: Variation of delay. The response with correct parameters is plotted in red. Green indicates that the real value is larger then that used for controller design, black marks the opposite.

Sliding mode control is more robust in view of parameter variation than control based upon linearized subsystems; it features consideration of parameter uncertainties $\tilde{\mathbf{M}}_{\mathbf{x}} = \hat{\mathbf{M}}_{\mathbf{x}} - \mathbf{M}_{\mathbf{x}}$, $\tilde{\mathbf{C}}_{\mathbf{x}} = \hat{\mathbf{C}}_{\mathbf{x}} - \mathbf{C}_{\mathbf{x}}$ and $\tilde{\boldsymbol{\eta}}_{\mathbf{x}} = \hat{\boldsymbol{\eta}}_{\mathbf{x}} - \boldsymbol{\eta}_{\mathbf{x}}$ in design. For a detailed analysis see (Slotine, 1985) where one can see that sliding mode control guarantees robustness against parameter uncertainties in case of integral action and is more robust than control schemes based upon linearization techniques.

6. Experimental results

For experimental evaluation, controller designs are implemented to the planar parallel manipulator FIVEBAR. For the sake of clarity a selection of the control schemes and design parameters presented in section 4 has been made. The focus is on centralized and

decentralized control (with optimized parameters) and its comparison to disturbance observer based control via input balancing. Sliding mode control with integral action is presented as nonlinear control scheme to compare nonlinear design performance to linearization techniques based ones.

6.1 Experimental setup and performance criteria

For control purposes the concept of skill primitives is used. The main idea consists of specifying a task and a terminating condition that lead to execution of next skill primitive. We here use the position accuracy ε_{pos} as terminating condition for each axis separately.

Workspace of the parallel robot FIVEBAR is illustrated in fig 13. A common trajectory for all setups is used to guarantee comparable results. The selected path covers the workspace almost completely, including positions close to singularities. It consists of 6 parts, each resembled by a skill primitive. The trajectory is generated piecewise and terminates with both axes fulfilling specified position accuracy.

For evaluation of controller performance different criteria are used: Concerning tracking error, a time-integral of absolute tracking error (ITAE) $\Delta_{t,\mathbf{x}_i}$ is used. It is defined for each axis in Cartesian coordinates,

$$\Delta_{t,\mathbf{x}_i} = \int_{t_0}^{t_1} \left| \mathbf{x}_{i,\text{ref}} - \mathbf{x}_{i,\text{act}} \right| \mathrm{d}t \tag{33}$$

respectively and gives a benchmark of in-time execution of trajectory.

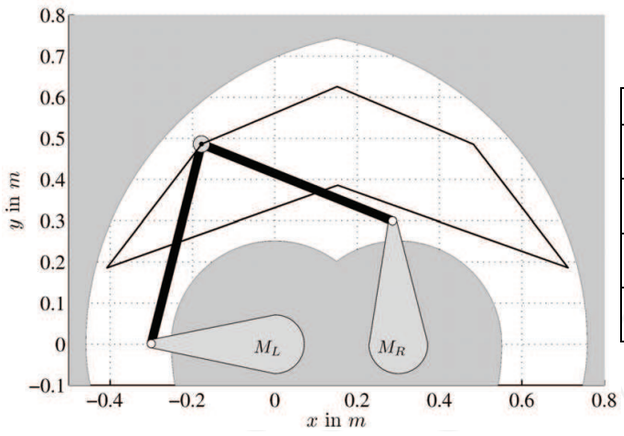

Specification of trajectory		
Velocity	$\lvert\dot{\mathbf{x}}\rvert_{\max}$	2 *m/s*
Acceleration	$\lvert\ddot{\mathbf{x}}\rvert_{\max}$	40 *m/s²*
Jerk	$\lvert\dddot{\mathbf{x}}\rvert_{\max}$	600 *m/s³*
Position accuracy	ε_{pos}	300 μm

Fig. 13: Workspace and experimental setup of FIVEBAR in initial position

Secondly, a position-integral of absolute Cartesian distortion (IACD) Δ_{A} is defined for benchmarking path-accuracy in operational space

$$\Delta_{\text{A}} = \oint_{x_{\text{ref}}} \left| y_{\text{ref}}(x_{\text{ref}}) - y_{\text{act}}(x_{\text{ref}}) \right| \mathrm{d}x_{\text{ref}} \tag{34}$$

It represents the absolute size of distortion areas and thus indicates accuracy of the end effector path with respect to the trajectory.

Moreover, settling time

$$t_{\text{settling}} = t_{\text{nextSKP}} - t_{\text{endSKP}} \tag{35}$$

is considered, where t_{endSKP} denotes time when the actual skill primitive ends and t_{nextSKP} represents the point of next skill primitive starting. They are defined by

$$\left|\tilde{\mathbf{x}}_i(t \geq t_{\text{nextSKP}})\right| \leq \varepsilon_{\text{pos}}\,, \quad t_{\text{endSKP}} = t \,|\, \left(\left|\dot{\mathbf{x}}_{\text{ref}}\right| = 0 \wedge \left|\ddot{\mathbf{x}}_{\text{ref}}\right| = 0\right) \tag{36}$$

In addition maximum tracking error $\Delta_{\text{trk},i}$ and maximum overshooting during settling time $\Delta_{\text{set},i}$ defined by

$$\begin{aligned} \Delta_{\text{trk},i} &= \max\left\{\left|\tilde{\mathbf{x}}_i(t)\right|\right\}, \quad t \in \{t_{\text{nextSKP}} \ldots t_{\text{endSKP}}\} \\ \Delta_{\text{set},i} &= \max\left\{\left|\tilde{\mathbf{x}}_i(t)\right|\right\}, \quad t \in \{t_{\text{endSKP}} \ldots t_{\text{nextSKP}}\} \end{aligned} \tag{37}$$

are evaluated.
Performance criteria could easily be extended – selected set is sufficient for an overview of performance instead of a claim to be overarching.

6.2 Data presentation

Plots of experimental results and data concerning trajectory are given in fig. 15-19, and used for benchmarks in the following.
It can be seen that overshooting during trajectory follow up is in general of higher value than during settling time, due to chosen high dynamics. Examining average settling time on centralized and decentralized control reveals that disturbance observers improve this property as expected by theoretical analysis in section 5. Furthermore maximum overshooting during trajectory follow up is reduced, which is also reflected in Cartesian distortion error, cf. fig. 14(b).

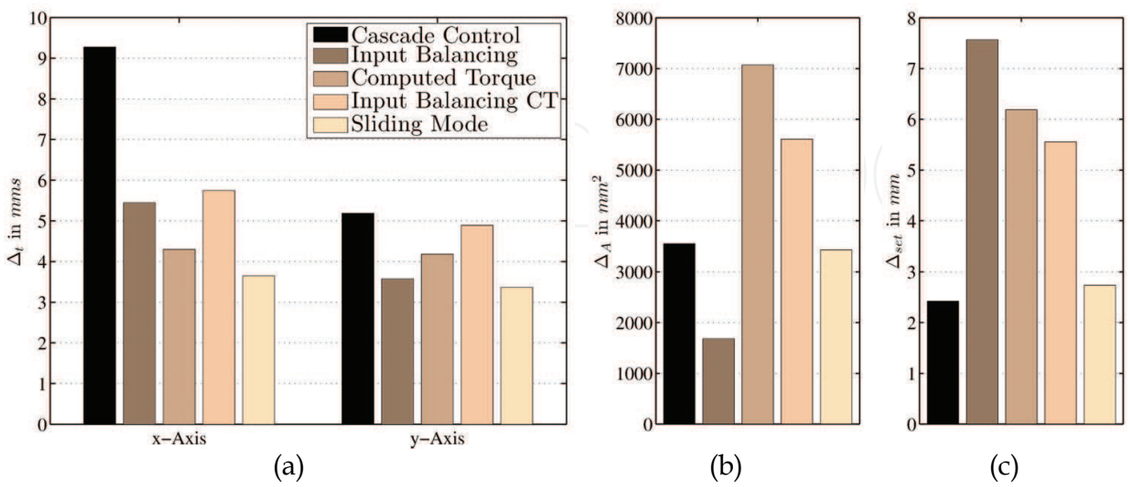

Fig. 14: Time integral of tracking error (a), Cartesian distortion (b) and maximum overshooting during settling time (c)

In comparing both linearization techniques with respect to Cartesian distortion, cf. fig. 14(a), and maximum overshooting during settling time, cf. fig. 14(c), it can be seen that cascade control with exact feedback linearization seems of better quality than computed torque control. The reason can be found in focus of control. While cascade control is operating in Cartesian space, computed torque addresses joint space. Thus an appropriate error in joint space is nonlinear (depending on position) transformed into Cartesian space.
Concerning nonlinear control design it can be seen that sliding mode control exhibits an overall up to best performance. All criteria except settling time range in high performance being only outperformed by input balancing concerning Cartesian distortion (fig. 14(b)). This is met by a far lesser overshooting during settling time (fig 14(c)) which substantiates the performance of sliding mode control. Due to inclusion of uncertainties in design its disturbance rejection during trajectory following up equals observer performance via input balancing. Its advantage compared to linear based controller design lies within its robustness against model uncertainties. As seen in section 5, linear design – especially input balancing – is more sensitive to variation of parameters, cf. fig. 11. This leads to loss of damping and can clearly be seen in settling times here (fig. 16). Input balancing shows large values in overshooting, indicating a parameter mismatch, while sliding mode control with same model-parameters offers far less overshooting. However, problems in positions close to workspace boundaries arise, which are indicated by a longer settling time after trajectory part 3 and 5, cf. fig. 19. In case of linear control schemes on the contrary these positions do not seem to have a significant impact on settling time, cf. fig. 15-18. The reasons can be found in nonlinear design, resulting in nonlinear closed loop dynamics and in design of sliding surface dynamics with integral action. Therefore a higher average settling time in case of sliding mode control can be seen. However, on other parts of the trajectory settling time is smaller than in case of all other control schemes.

	x	y
Δ_{trk}	10.7 *mm*	7.8 *mm*
Δ_{set}	1.7 *mm*	2.4 *mm*
$\bar{t}_{\text{settling}}$	0.75 *s*	

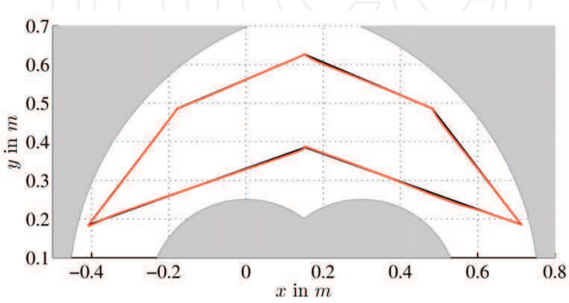

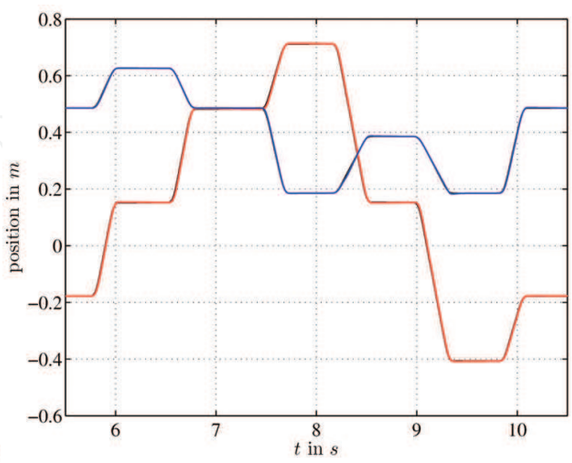

Fig. 15: Experimental Results on cascade control

	x	y
Δ_{trk}	8.1 *mm*	7.2 *mm*
Δ_{set}	7.6 *mm*	6.4 *mm*
$\bar{t}_{\text{settling}}$	0.43 *s*	

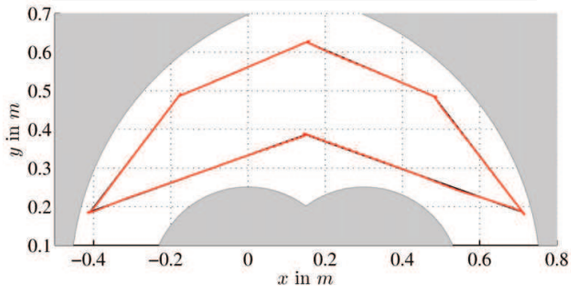

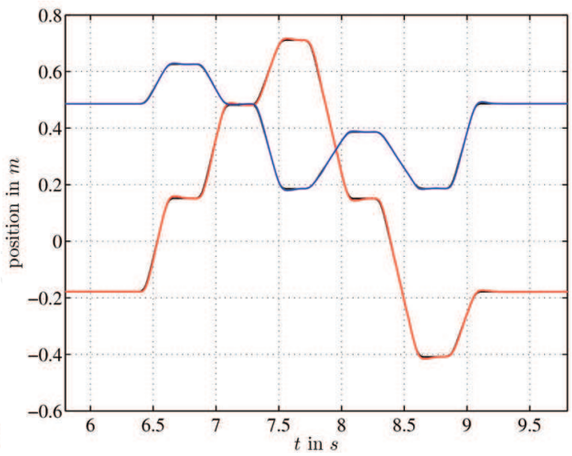

Fig. 16: Experimental Results on input balancing

	x	y
Δ_{trk}	14.2 *mm*	9.4 *mm*
Δ_{set}	1.6 *mm*	6.2 *mm*
$\bar{t}_{\text{settling}}$	0.91 *s*	

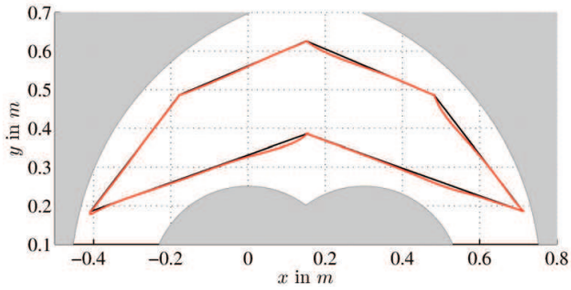

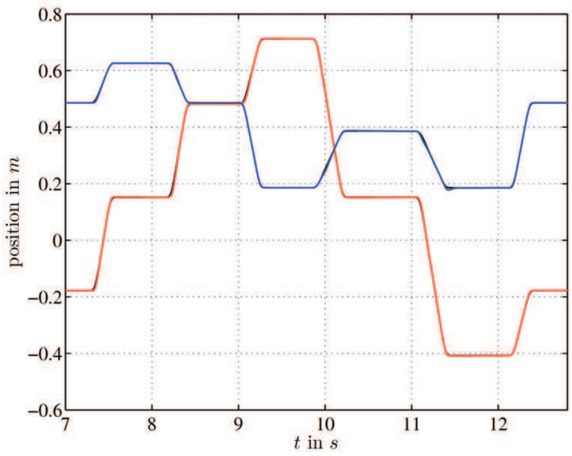

Fig. 17: Experimental Results on computed torque control

	x	y
Δ_{trk}	12.9 *mm*	9.7 *mm*
Δ_{set}	5.5 *mm*	2.8 *mm*
$\bar{t}_{\text{settling}}$	0.67 *s*	

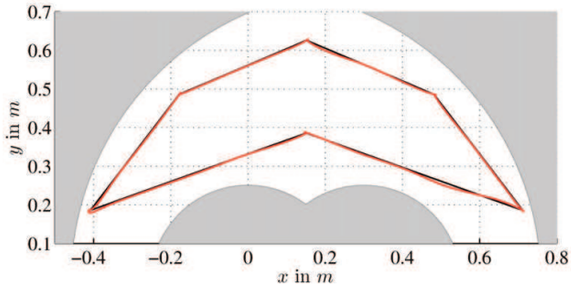

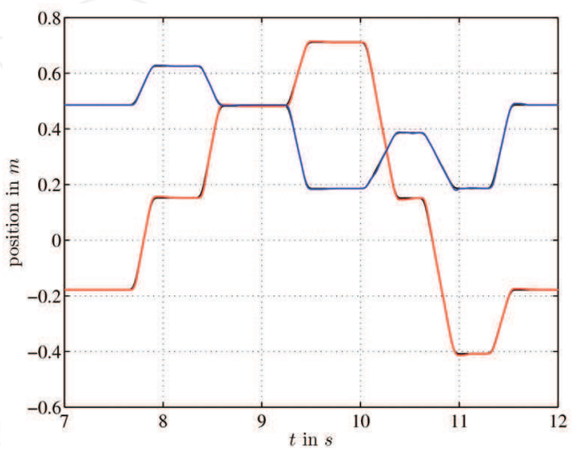

Fig. 18: Experimental Results on computed torque with input balancing

	x	y
Δ_{trk}	3.9 *mm*	6.6 *mm*
Δ_{set}	2.7 *mm*	1.8 *mm*
$\bar{t}_{settling}$	3.37 *s*	

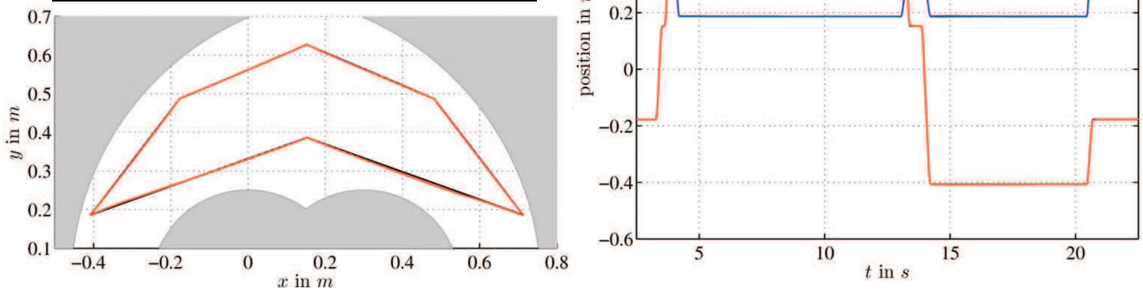

Fig. 19: Experimental Results on sliding mode control

Towards chattering associated with sliding mode control the continuous control lessens this tendency as can be seen in fig. 20. Here a single drive torque during a trajectory part is compared to cascade control. Although frequency analysis reveals energy in frequencies next to the characteristic ones of cascade control, it can be seen that these are damped well in contrast to classical sliding mode control with discontinuous control law.

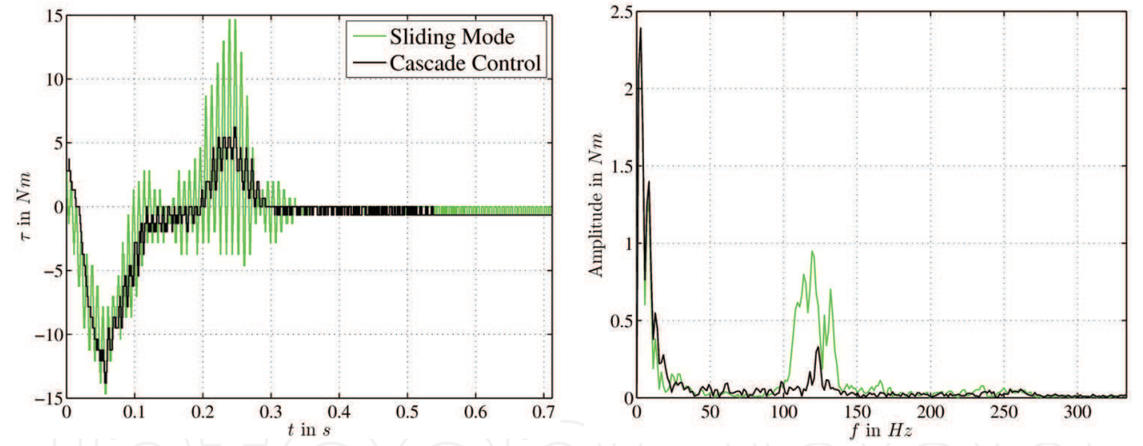

Fig. 20: Comparison of torques of linear and nonlinear design

Comparing presented results it can be seen that each control scheme features specific advantages, cf. tab. 2. The performance of each controller lies within its concept of design. Centralized, i.e. cascade control with feedback linearization guarantees tracking whereas disturbance rejection is not explicitly included in design process. Thus parameter uncertainties in modeling result in cross coupling of axes by inverse dynamic control scheme, cf. eq. (12) and (13). This can be matched by use of disturbance observers as the concept of input balancing, reducing Cartesian distortion and time integral of tracking error. As a drawback, however, a parameter mismatch leads to a loss of damping resulting in a higher overshooting during settling time. This can be improved by explicitly considering model- and parameter-uncertainties via sliding mode control at the cost of position dependent settling dynamics.

Decentralized, i.e. computed torque control reveals a good performance, and becomes handy when the direct kinematic problem is not computational efficient anymore. For control concepts considering wide range parameter variation other concepts have to be focused – such as adaptive control, which is discussed in (Hesselbach et al., 2004) with experimental benchmarking.

	CC	CT	IB	SMC
Path accuracy	+	o	++	+
Tracking	o	+	+	++
Axis coupling	-	-	-	+
Robustness against model uncertainties	o	o	-	+
Disturbance rejection	o	o	+	++
Axis independent design	+	o	+	+
Velocity noise	+	++	++	o
Chattering	++	++	+	o
Execution time	+	o	++	- (++)

Tab. 2: Properties of different control approaches: CC – cascade control, CT – computed torque control, IB – input balancing, SMC – sliding mode control

7. Conclusion

Different model based control architectures have been analyzed and compared by experimental studies. Experiments were carried out on a planar parallel robot optimized for high-speed operation.

Starting with a generalized scheme for discrete modeling of parallel structures, design of controllers are given at hand and discussed with respect to performance and robustness. Performance of each control design was analyzed and compared. In experimental results design concepts are validated, revealing that sliding mode control is a promising alternative to classical linear design concepts on parallel robots. Its main advantage is explicit inclusion of uncertainties to the design of the controller, whereas centralized and decentralized control just consider the nonlinearities on the innermost level.

Control by sliding surfaces demands a trajectory specified in position, velocity and acceleration. In the fields of robotics, however, providing a full trajectory is no real restriction, because these are planned jerk-bounded to prevent the mechanical structure from being damaged.

Nonetheless centralized and decentralized control feature certain advantages. Computed torque control is the best solution in case of complex direct kinematics, guaranteeing real-time execution. Best suppression of noisy velocity signals is featured since these do not influence the feedforward-linearization. Centralized control provides good path accuracy and is worth to be extended by input balancing in case of absence of parameter uncertainties improving Cartesian distortion. It is optimized towards disturbance rejection, however lacks robustness against parameter uncertainties.
In case of large parameter variations – for example caused by payloads – presented methods can be extended to parameter adaption, which sliding mode control and computed torque control fit best for.

8. Acknowledgements

This work was funded by the German Research Foundation (DFG) within the framework of the Collaborative Research Center SFB 562 "Robotic Systems for Handling and Assembly". We would like to thank QNX for providing licenses of the real-time operating system.

9. References

Bohn, C. (2000), Recursive parameter estimation for nonlinear continuous-time systems through sensitivity model-based adaptive filters, Ph.D. dissertation, Ruhr-Universität Bochum, 2000.

Brandenburg, G.; Papiernik, W. (1996). Feedforward and Feedback Strategies Applying the Principle of Input Balancing for Minimal Tracking Errors in CNC Machine Tools, Proc. of 4th International Workshop on Advanced Motion Control (AMC '96), pp. 612-618 vol.2., Mie, March 1996, Japan.

Brunotte, Ch. (1999). Regelung und Identifizierung von Linearmotoren fuer Werkzeugmaschinen, Ph.D. dissertation, University of Braunschweig (in German).

Dizioglu, B. (1966). Getriebelehre. Bd. 3. Dynamik. Vieweg, Braunschweig (in German).

Filippov, A.F. (1988). Differential equations with discontinuous right-hand sides, Springer, ISBN: 978-9027726995, Netherlands.

Finkemeyer, B. (2004). Robotersteuerungsarchitektur auf Basis von Aktionsprimitiven, Ph.D. dissertation, University of Braunschweig (in German).

Hesselbach, J.; Pietsch, I.T., Bier, C.C, Becker, O.T. (2004). Model-based Control of Plane Parallel Robots – How to Choose the Appropriate Approach?, *Proc. of 4th Chemnitz Parallel Kinematics Seminar (PKS2004)*, pp. 211-231, Chemnitz, April 2004, Germany.

Isidori, A. (1995). Nonlinear Control Systems, Springer, ISBN: 978-3540199168, London.

Kock, S. (2001). Parallelroboter mit Antriebredundanz, Ph.D. dissertation, Fortschritt-Berichte VDI, Duesseldorf – Braunschweig (in German).

Kolbus, M.; Reisinger, T.; Maaß, J. (2005). Robot Control Based on Skill Primitives, Proc. of IASTED Conf. on Robotics and Applications, pp. 260-266, Camebridge, October 2005, USA.

Leonhard, W. (1996). Control of Electrical Drives, Springer, ISBN: 978-3540418207, Berlin – Heidelberg - New York.

Levant, A.; Friedman, L. (2002). Higher Order Sliding Modes, In: Sliding Mode Control in Engineering (Control Engineering Series, 11), Perruquetti, W.; Barbot, J.-P. pp. 53-101, Marcel Dekker, Inc., ISBN: 978-0824706715, New York.

Luenberger, D.G. (1964). Observing the state ov a linear system, IEEE Transactions on Military Electronics, pp. 74-80.

Lunze, J. (2006). Regelungstechnik 2: Mehrgrößensysteme, Digitale Regelung, Springer, ISBN: 978-3540323358, Berlin

Merlet, J.-P. (2000). Parallel Robots, Kluwer Academic Publishers, Springer, ISBN: 978-1402041327, Netherlands.

Murray, R.M., Li, Z., Sastry, S.S. (1994), A mathematical introduction to robotic manipulation. CRC Press LLC, ISBN: 978-0849379819, USA.

Nakamura, Y. (1991). Advanced robotics: redundancy and optimization, Addison-Wesley Publishing Company, Inc., ISBN: 978-0201151985.

Sciavicco, L.; Siciliano, B. (2001). Modelling and Control of Robot Manipulators, Springer, ISBN: 978-1852332211, Berlin.

Stachera, K.; Schumacher, W. (2007). Simultaneous calculation of the direct dynamics of the elastic parallel manipulators, Proc. of the 13th IEEE IFAC International Conference on Methods and Models in Automation, pp. 863-868, Szczecin, August 2007, Poland.

Stachera, K.; Wobbe, F.; Schumacher, W. (2007). Jacobian-based derivation of dynamics equations of elastic parallel manipulators, Proc. of the IASTED Asian Conference on Modelling and Simulation (AsiaMS 2007), pp. 47-54, Beijing, October 2007, China.

Spong, M. W.; Vidyasagar, M. (1989). Robot dynamics and control, John Wiley & Sons, Inc., ISBN: 978-0471612438, USA.

Slotine, J.-J. (1983). Tracking Control of Nonlinear Systems Using Sliding Surfaces, Doctoral Dissertation, Massachusetts Institute of Technology.

Slotine, J.-J. (1985). The Robust Control of Robot Manipulators, International Journal of Robotics Research, vol. 4, no. 2, pp. 49-64, 1985.

Slotine, J.-J.; Li, W. (1991). Applied Nonlinear Control, Prentice Hall, ISBN: 978-0130408907, New Jersey.

Tsai, L.-W. (1999), Robot Analysis, Wiley-Interscience; ISBN: 978-0471325932, New York.

Utkin, V.I. (1977). A Survey: Variable Structure Systems with Sliding Modes, IEEE Transactions on Automatic Control , vol. 22, no. 2, pp. 212-222, April 1977.

Vetter, W. (1973). Matrix calculus operations and taylor expansions, SIAM Review, vol. 15, pp. 352–369, 1973.

Weinmann, A. (1991).Uncertain mod and robust control, Springer, ISBN: 978-3-211-82299-9, Wien.

Whitcomb, L.L.; Rizzi, A.; Koditschek, D.E. (1993), Comparative Experiments with a New Adaptive Controller for Robot Arms, IEEE Transactions on Robotics and Automation, vol. 9, no. 1, pp 59-70, Februar 1993.

Wobbe, F.; Schumacher, W.; Böske, W. (2006). Optimierte Antriebsreglerstrukturen zur Störunterdrückung, SPS/IPC/DRIVES 2006, Nürnberg (in German)

Wobbe, F.; Kolbus, M.; Schumacher, W. (2007). Continuous Sliding Surfaces versus Classical Control Concepts on Parallel Robots, Proc. of the 13th IEEE IFAC International Conference on Methods and Models in Automation, pp. 869–874, Szczecin, August 2007, Poland.

Automation and Robotics

Edited by Juan Manuel Ramos Arreguin

ISBN 978-3-902613-41-7
Hard cover, 388 pages
Publisher I-Tech Education and Publishing
Published online 01, May, 2008
Published in print edition May, 2008

In this book, a set of relevant, updated and selected papers in the field of automation and robotics are presented. These papers describe projects where topics of artificial intelligence, modeling and simulation process, target tracking algorithms, kinematic constraints of the closed loops, non-linear control, are used in advanced and recent research.

InTech Europe
University Campus STeP Ri
Slavka Krautzeka 83/A
51000 Rijeka, Croatia
Phone: +385 (51) 770 447
Fax: +385 (51) 686 166
www.intechopen.com

InTech China
Unit 405, Office Block, Hotel Equatorial Shanghai
No.65, Yan An Road (West), Shanghai, 200040, China
中国上海市延安西路65号上海国际贵都大饭店办公楼405单元
Phone: +86-21-62489820
Fax: +86-21-62489821

IntechOpen